PCCP

Accepted Manuscript

This article can be cited before page numbers have been issued, to do this please use: M. J. Eslamibidgoli, A. Gross and M. Eikerling, *Phys. Chem. Chem. Phys.*, 2017, DOI: 10.1039/C7CP03396F.

ROYAL SOCIETY OF CHEMISTRY

rsc.li/pccp

View Article Online
DOI: 10.1039/C7CP03396F

Surface configuration and wettability of nickel (oxy)hydroxides: a first-principles investigation

Mohammad Javad Eslamibidgoli[a,b], Axel Groß[b,*], and Michael Eikerling[a]

[a] Department of Chemistry, Simon Fraser University, 8888 University Drive, Burnaby, V5A 1S6, BC, Canada

[b] Institute of Theoretical Chemistry, Ulm University, Albert-Einstein-Allee 11, D-89069 Ulm, Germany

ABSTRACT

This article explores the wetting behavior of β-type nickel hydroxide, β-$Ni(OH)_2$, and nickel oxyhydroxide, β-NiOOH, by means of first-principles calculations. Water is found to interact weakly with β-$Ni(OH)_2$ (001), but strongly with β-NiOOH (001). As unveiled with the use of *ab initio* molecular dynamics simulations, surface water layers at β-NiOOH (001) show a high degree of ordering correlated with a large surface polarization effect. In comparison, interfacial water at β-$Ni(OH)_2$ (001) exhibits enhanced disorder and higher mobility. The weak interaction of water with β-$Ni(OH)_2$ (001) is consistent with the small dipole moment of this surface. On the surface of β-NiOOH (001), in addition to the significantly increased surface dipole moment, unsaturated O atoms increase the number of hydrogen bonds between water molecules and surface, resulting in strong water binding. The wettability trends found in this simulation study is consistent with experimental observations. Another theoretical observation is the increased work function of β-NiOOH (001) relative to β-$Ni(OH)_2$ (001) that agrees with experimental results reported in the literature.

KEYWORDS: nickel (oxy)hydroxides, solid-electrolyte interface modeling, surface wettability, DFT calculations, *ab initio* molecular dynamics

View Article Online
DOI: 10.1039/C7CP03396F

1. INTRODUCTION

Hydrogen is the most promising fuel to fulfill the demands of a clean and sustainable energy society in view of vehicle propulsion and large-scale energy storage [1]. Neat hydrogen can be produced by alkaline water electrolysis, which uses electrical energy to split water molecules into oxygen and hydrogen [2]. In these electrochemical cells, the anodic oxygen evolution reaction is especially challenging because it consumes a large amount of the available Gibbs energy, thereby diminishing the overall system efficiency [3]. A major focus of research forays in this field lies, therefore, on the development of efficient electrocatalyst materials to reduce these energy losses [4,5].

Nickel-based (oxy)hydroxides, as earth-abundant materials, have seen a recent surge of interest as electrocatalysts for water splitting in alkaline conditions [6,7]. While the use of these materials in battery electrodes dates back to the last century [8,9], the renewed focus is mainly incited by the advancement of experimental techniques that are suitable to explore structural and electrochemical properties of these materials [10,11,12].

In the late 1960s, a seminal X-ray diffraction study by Bode revealed four main phases of Ni (oxy)hydroxide. They include two phases of Ni hydroxide, labeled as α- and β-$Ni(OH)_2$, and two phases Ni oxyhydroxide, referred to as β- and γ-NiOOH [13]. Cyclic voltammetry (CV) was employed to study oxidation and reduction processes at a Ni(poly) electrode in 0.5 M aqueous KOH solution at T = 293 K [14,15,16]. Potential cycling between 0.50 and 1.55 V vs. RHE at a scan rate $\nu = 100$ mV s^{-1} was seen to trigger the phase transition from β-$Ni(OH)_2$ to β-NiOOH and back. The anodic and cathodic peaks associated with these transitions were observed at 1.45 and 1.36 V vs. RHE, respectively. For cycling to lower potentials the formation and reduction of α-$Ni(OH)_2$ was observed, with anodic and cathodic peaks at 0.30 and −0.05 V vs. RHE, respectively [16].

The atomic structure of Ni (oxy)hydroxide phases consist of NiO_2 slabs with tetrahedral coordination of hydrogen atoms in the inter-slab space, as shown in Fig. 1 (a) and (b). The crystal structure of bulk β-

View Article Online
DOI: 10.1039/C7CP03396F

$Ni(OH)_2$ is isostructural with brucite, with the space group $P\bar{3}m1$ and lattice parameters a = b = 3.126 Å and c = 4.605 Å [17,18,19]. On the other hand, the atomic structure of bulk β-NiOOH is still debated [20,21]. Controversy evolves around possible stacking orders of the layers as well as the location of hydrogen atoms within the structure [21]; α- and γ-phases are based on β-phases, but they also involve intercalated water molecules (and other ionic species) with varying degree of hydration [9].

The renewed focus on Ni-based oxides as efficient catalyst materials for water splitting has stimulated a flurry of theoretical investigations using quantum mechanical simulations [20,21,22,23,24,25,26,27]. These efforts, mostly at the level of DFT + U, strived to rationalize the thermodynamic stability of the various bulk phases of NiO_x-based materials [21,27], the relative stability of various surface terminations [20,26], their electronic properties [20,21,26], and the resulting electrocatalytic activity for the OER [22,23,24,25]. Surface calculations on Ni oxyhydroxides have focused on the $(01\bar{1}5)$ or similar facets, which was justified by the higher OER activity expected for such planes [22,23,24,25]. On the other hand, X-ray diffraction (XRD) studies showed the highest intensity for the (001) surface facet [9]. As well, DFT + U calculations of various low-index surfaces of β-$Ni(OH)_2$ and β-NiOOH predicted the highest thermodynamic stability for the (001) surface [20]. Therefore, it seems expedient to focus on the (001) surface for detailed computational studies of interrelated surface properties as well as the mechanism and pathway of the OER.

Despite major progress in the field of first-principles electrochemistry, fundamental understanding about the processes taking place at the electrode-electrolyte interface is still incomplete [28]. This is due to the fact that the self-consistent theoretical treatment of structure, properties and reactions at solid-liquid interfaces requires a proper accounting for the electrolyte, which in turn demands computationally demanding statistical averaging [28, 29]. It is well known that the surficial water molecules play an important role in reaction pathways of electrochemical processes [30, 31, 32, 33, 34, 35, 36, 37]. The binding energy and configuration of interfacial water affect the work function and the electrostatic

View Article Online
DOI: 10.1039/C7CP03396F

charging properties of the surface [29, 38]. Moreover, surficial water molecules play a vital role for the reaction kinetics, as donor or acceptor species for protons or hydroxide ions needed to complete electrochemical surface reactions.

This contribution provides insights into the molecular-level interactions and configurational ordering of surficial water at (001) facets of Ni (oxy)hydroxides; it serves a broader goal to understand the impact of the electrochemical environment on the OER. We present results of first-principles calculations at the level of DFT + U, performed to study water adsorption on β-$Ni(OH)_2$ (001) and β-NiOOH (001) surfaces. We discuss the impact of water adsorption on the electronic structure and charging properties of these surface facets. *Ab initio* molecular dynamics (AIMD) simulations were performed to account for thermal fluctuations in ordering of surficial water at Ni (oxy)hydroxides (001). This computational study expands the scope of similar studies on water/transition metal interfaces [29,39,40,41,42,43,44,45] towards water/oxides surfaces.

2. COMPUTATIONAL METHODS

Calculations reported here have been performed with the Vienna *Ab initio* Simulation Package (VASP) [46,47]. The ionic cores were represented by projected augmented waves (PAW) [48]. Kohn−Sham one-electron wave functions were expanded in a plane wave basis set with an energy cutoff of 500 eV. Exchange and correlation effects were incorporated within the generalized gradient approximation (GGA) to describe the exchange–correlation effects, using the Perdew, Burke and Ernzerhof (PBE) exchange–correlation functional [49]. Due to incomplete cancellation of Coulomb self-interaction, plain DFT functionals do not capture the electronic structure of these materials with sufficient accuracy [50]. Inclusion of the Hubbard-U term within the DFT + U approach corrects the electronic structure of Ni. This approach improves the treatment of on-site Coulomb interactions for the d-orbitals. We employed the spin-polarized DFT+U approach of Dudarev *et al*. [51] with a U−J parameter of 5.5 eV; this value

View Article Online
DOI: 10.1039/C7CP03396F

was taken from the work of Li and Selloni [22], where it was calculated using linear response theory [52].

Bulk structures of NiO_x materials used in our simulations are based on the study of Van der Ven *et al*. [53]. β-$Ni(OH)_2$ has the ABAB oxygen stacking sequence (called T1, also see Fig. 1 (a)), and β-NiOOH has AABBCC oxygen stacking sequence (called P3) [53]. In the latter case, as shown in Fig. 1 (b), hydrogen atoms present in the inter-layer space create a saturated number of hydrogen bonds between the layers. In fact, as also stated in Ref. [20], infrared spectroscopy measurements suggest that β-NiOOH is a hydrogen-bonded structure with no free hydroxyl groups [8,55]. Bulk β-NiOOH was represented as a model system with a $1 \times 2 \times 1$ unit cell.

A geometry relaxation was performed with a $6 \times 6 \times 4$ Γ-point-centered Monkhorst−Pack k-point mesh [54] and a force threshold of 0.01 eV/Å. The optimized structures obtained as well as the corresponding unit cell parameters are shown in Fig. 1 (a) and (b).

Having obtained bulk structures, surface configurations were modeled as three-layer slabs of β-$Ni(OH)_2$ (001) or β-NiOOH (001) with $2\sqrt{3} \times 2\sqrt{3}$-R30° or 3×4 unit cells. These unit cell configurations are commensurate with the addition of water layers and they allow varying surface terminations for β-NiOOH (001) to be created (see Fig 1 (c), (d) and (e)). All model structures include 12 Ni atoms, 24 O atoms, as well as 24 and 12 H atoms per layer of the slab for β-$Ni(OH)_2$ (001) and β-NiOOH (001), respectively. Only the Ni atoms of the bottom layer were fixed at their bulk positions.

β-$Ni(OH)_2$ (001) has only one possible surface termination with 100% OH^{ad} (Fig. 1 (c)). On the other hand, depending on the choice of unit cell, three different surface terminations of β-NiOOH (001) can be generated, with (i) 25% OH^{ad} and 75% O^{ad} (Fig. 1 (d)), $NiOOH_{25/75}$ (001), for the $2\sqrt{3} \times 2\sqrt{3}$- R30° unit cell, (ii) with 50% OH^{ad} and 50% O^{ad} (Fig. 1 (e)), $NiOOH_{50/50}$ (001), for the 3×4 unit cell, and (iii) 75% OH^{ad} and 25% O^{ad} (Fig. 1 (f)), $NiOOH_{75/25}$ (001), again for the $2\sqrt{3} \times 2\sqrt{3}$- R30° unit cell. To

View Article Online
DOI: 10.1039/C7CP03396F

simulate the effect of surficial water, the surface coverage of water was changed step-wise from 0 ML to 1 ML on β-$Ni(OH)_2$ (001) and from 0 ML to 5/6 ML on β-NiOOH (001).

The maximum water coverages of 1 ML at β-$Ni(OH)_2$ (001) and 5/6 ML at β-NiOOH (001) correspond to almost the same surface density of water molecules, i.e., 1.16 × 10^{15} cm^{-2} and 1.11 × 10^{15} cm^{-2}, respectively. At 2/3 ML the hexagonal ice-like water structure with H-down configuration has been usually used in our study, except for β- $NiOOH_{50/50}$ (001). In the latter case, the symmetry of the unit cell (i.e., 3×4) does not allow putting a water layer with hexagonal ice-like structure on the surface. For geometry optimizations of the slab models, we used 4 × 4 × 1 k-points, and a force threshold of 0.05 eV/Å.

AIMD simulations were performed in the microcanonical ensemble using the Verlet algorithm with a time step of 1 fs at a temperature of 140 K. This temperature was chosen as it is close to the typical desorption temperature of single water layers on metal electrodes [56]. The simulations were started using the configurations obtained from DFT-based energy minimization. Initially the mean kinetic energy was set to twice the targeted temperature of 140 K. We considered the water thermalization time to be ~1 ps when the mean kinetic energy dropped to about half the initial value. The number of k-points in the AIMD simulations was decreased to 2 × 2 × 1.

3. RESULTS AND DISCUSSION

The adsorption energy per water molecule on the slab surface is calculated as,

$$E_{ad} = \frac{1}{n}\left(E_{tot} - E_{slab} - nE_{H_2O}\right), \qquad (1)$$

where E_{tot}, E_{slab} and E_{H_2O} correspond to the energies of the NiO_x–water system, the bare NiO_x slab and the isolated water molecule, respectively; n is the number of water molecules per unit-cell.

A water monomer binds relatively weakly at β-$Ni(OH)_2$ (001). As shown in Table 1, among various possible configurations examined, it was found that a single water molecule binds more strongly in

View Article Online
DOI: 10.1039/C7CP03396F

between the triply coordinated OH groups with a "tilted" H-down configuration in order to form a hydrogen bond with the re-oriented OH^{ad}; this configuration is shown in Fig. 2 (a) and (e). In this case, the distance from the O atom in H_2O to the nearest Ni atom is d_{H2O-Ni} = 3.55 Å, and that to the nearest O atom in OH^{ad} is d_{H2O-OH} = 3.24 Å; the adsorption energy of water is -0.25 eV.

On the other hand, a water monomer binds strongly at the surface of β-NiOOH (001). Among various examined orientations shown in Table 1, it was found that on β- $NiOOH_{25/75}$ (001) a water monomer binds via its oxygen atom to OH^{ad} with d_{H2O-OH} = 2.70 Å, as can be seen in Fig. 2 (b) and (f), while it forms two more hydrogen bonds with O groups at the surface with d_{H2O-O} = 2.83 Å and d_{H2O-O} = 2.93 Å. The adsorption energy for a single water molecule at this surface is -0.45 eV. Similarly for β- $NiOOH_{50/50}$ (001), a single water molecule creates a hydrogen bond with OH^{ad}, while it forms another hydrogen bond with one O at the surface, as depicted in Fig. 2 (c) and (g). The adsorption energy in this case is -0.54 eV, while the distances between the water monomer and OH and O ar d_{H2O-OH} = 2.73 Å and d_{H2O-O} = 2.70 Å, respectively. For β- $NiOOH_{75/25}$ (001), a water monomer binds more strongly to O groups in H-down configuration, with d_{H2O-O} = 2.63 Å, while its O atom forms two more hydrogen bonds with two OH^{ad}. In this case, the adsorption energy was found to be -0.69 eV, which is larger as compared to water monomer adsorption for two other terminations, as seen Fig. 2 (d) and (h).

Therefore, a water monomer creates more hydrogen bonds with β-NiOOH (001) due to the fact that the surface is not saturated with hydrogen as in the case of β-$Ni(OH)_2$ (001). The increased number of hydrogen bonds leads to stronger water binding and smaller distances between the water monomer and β- NiOOH (001) surfaces as compared to β-$Ni(OH)_2$ (001).

As illustrated in Fig 3 (b), (h), (n), and (t), we increased the number of water molecules in the unit cell by adding the second molecule away from the first one at the surface. Obviously, due to the weak water-water interaction, in this case rather similar adsorption energies were obtained as for water monomer adsorption for each of the four considered surfaces (shown in Fig. 2). Focusing on water dimerization on

View Article Online
DOI: 10.1039/C7CP03396F

these surfaces, cf. Fig. 3 (c), (i), (o), and (u), we obtained the adsorption energies per water molecule to be -0.31 eV for β-$Ni(OH)_2$ (001), and -0.51 eV, -0.58eV, and -0.55 eV for β-NiOOH (001) with 25/75, 50/50 and 75/25 ratios of OH and O surface terminations, respectively. This means that water dimerization is favored for all terminations except for β- $NiOOH_{75/25}$ (001). The anomaly for β-$NiOOH_{75/25}$ (001) is due to the specific adsorption site for the water monomer, which results in a highly favored adsorption configuration.

For higher water density, illustrated in Fig. 3, adsorbed water molecules form a hydrogen-bonded network, further stabilizing the system. For the coverage of 2/3 ML, see Fig 3 (f), (i), (r), and (x), the adsorption energy per water molecule on β-$Ni(OH)_2$ (001) was found to be -0.44 eV, while that for β-NiOOH (001) surfaces was obtained as -0.69 eV, -0.64 eV and -0.71 eV, for terminations of 25/75, 50/50 and 75/25, respectively. We note the slightly smaller calculated adsorption energy for β-$NiOOH_{50/50}$ (001), which is due to the formation of an incomplete hexagonal structure, and consequently an incomplete hydrogen bond network, owed to the geometry of the unit-cell.

In order to separate water-NiO_x from water–water interactions, we performed an energy calculation for an isolated hexagonal water layer with all water molecules fixed in positions as in the configuration of the water layer when adsorbed on β-$Ni(OH)_2$ (001) or β- $NiOOH_{75/25}$ (001). The strength of water-water interactions can be calculated as [41],

$$\Delta E_{layer}^{H2O} = \frac{1}{n}(E_{water\ layer}^{isolated} - nE_{H2O}). \qquad (2)$$

where $E_{waterlayer}^{isolated}$ is the energy obtained for the isolated water layer. Still it should be noted that this separation is not exact as the water-water interaction on the surface becomes modified by the change of the electronic structure of the water molecules upon adsorption, however, this effect is typically small [57]. The calculated ΔE_{layer}^{H2O} for β-$Ni(OH)_2$ (001) is -0.33 eV, while that for β- $NiOOH_{75/25}$ (001) is -0.37 eV, which means the water-water interaction is stronger on β- NiOOH (001) surfaces. This

View Article Online
DOI: 10.1039/C7CP03396F

observation is due to the fact that the lattice constant for β-NiOOH is smaller by about 7.5% in comparison to β-$Ni(OH)_2$, resulting in a stronger interaction between neighboring water molecules on β-NiOOH (001). In summary for this part, we found stronger water-water, as well surface-water interactions on β-NiOOH (001), as compared to β-$Ni(OH)_2$ (001).

Next, as also studied in Ref. [58] for a number of transition metal surfaces, the adsorption energies of water in hexagonal arrays on β-$Ni(OH)_2$ (001) and β-NiOOH (001) surfaces were compared to the lattice energy of the hexagonal phase of bulk ice in order to evaluate the wettability. As can be seen in Fig. 4, the adsorption of water on β-$Ni(OH)_2$ (001) is much weaker than the lattice energy of bulk ice. This is an indication of the more hydrophobic nature of this surface. On the other hand, water adsorption on β-NiOOH (001) is similar to the lattice energy of bulk ice. Moreover, the trend obtained for the calculated adsorption energies of water on β-$Ni(OH)_2$ (001) and β-NiOOH (001) is similar to that Ag(111) and Au(111), as examples of hydrophobic surfaces, and on Pd(111) and Pt(111), as examples of hydrophilic surfaces, respectively (see Ref. [58]).

In order to understand the origin of the differences in water adsorption on β-$Ni(OH)_2$ and β-NiOOH (001), we determined the electron density difference of surfaces of NiO_x with varying surface terminations in vacuum (Fig. 5). The electron density difference along z direction was calculated as,

$$\Delta\lambda\,(z) = \iint \rho_{diff}\,dxdy. \qquad (3)$$

where, $\rho_{diff} = \rho_{NiOx} - (\rho_{Ni} + \rho_{Ox})$, is the difference between the electron density of one NiO_x layer and the sum of the separately calculated electron densities of non-interacting Ni atoms and O (or OH) at their same atomic positions in the NiOx layer.

Given $\Delta\lambda(z)$ the absolute value of surface dipole moment for a 2D configuration can be calculated as

$$|\mu_{surf}(LHS)| = |\int_{-vac}^{Ni\ site} z\,\Delta\lambda\,(z)dz\,|, \qquad (4)$$

View Article Online
DOI: 10.1039/C7CP03396F

or

$$|\mu_{surf}(RHS)| = |\int_{Ni\ site}^{+vac} z\,\Delta\lambda\,(z)dz|, \qquad (5)$$

for the "left hand side" (LHS) or the "right hand side" (RHS) of the surface. Here, *-vac* and *+vac* denotes the position in vacuum, at which the electron density vanishes on the relevant side of the 2D surface.

Fig. 5 shows the calculated electron density difference profiles, as well as dipole moments of various NiO_x surfaces. As shown in Fig. 5 (a), the symmetric configuration of OH^{ad} on both sides of β-$Ni(OH)_2$ (001) results in symmetric electron density difference profile with electron depletion regions at Ni atoms and electron buildup regions at O atoms of OH^{ad}; the calculated surface dipole moment for β-$Ni(OH)_2$ (001) was found to be 0.19 D for each side of the surface. As shown in Fig. 5 (b), the profile for β-$NiOOH_{50/50}$ (001) is also symmetric due to symmetric adsorbate configurations. However, the dipole moment was increased to 1.10 D for each side of this surface. For β- $NiOOH_{25/75}$ (001) or β- $NiOOH_{75/25}$ (001), as shown in Fig. 5 (c), the calculated dipole moments were also still larger comparing to that for β-$Ni(OH)_2$ (001).

Given that in a slab configuration water interacts only with one side of the studied 2D surface models, we can conclude that, in addition to the site specific adsorption and increased number of hydrogen-bonds between water molecules and β-NiOOH (001), the large surface dipole moment of β-NiOOH (001) adds to the strong interaction with surficial water molecules. On β-$Ni(OH)_2$ (001) this dipole-dipole interaction is much weaker due to the smaller surface dipole moment.

Fig. 6 shows the electron density difference upon water adsorption on these surfaces, which corresponds to the adsorption-induced charge rearrangement. As can be seen by comparing Fig 6 (a) and (b), the charge polarization caused by water adsorption on β-$Ni(OH)_2$ (001) is significantly smaller than

View Article Online
DOI: 10.1039/C7CP03396F

that for β-NiOOH (001), confirming the weaker interaction between water and β-$Ni(OH)_2$ (001). On β-NiOOH (001) there is a significant electron accumulation, indicated as yellow zones in Fig. 6 (b), below the flat-lying water molecules, which induces electron depletion zone on OH^{ad} (shown as blue zones). Additionally, there are electron depletion zones below the water molecules in H-down configuration, which induce electron accumulation on the O atoms at the surface. On the other hand, in comparison to β-NiOOH (001) water adsorption on β-$Ni(OH)_2$ (001) does not incur a significant electron density rearrangement, as revealed by Fig 6 (c) and (d).

Fig. 7 shows the one-electron potential distribution in the direction normal to the surface for the β-$Ni(OH)_2$ and β-NiOOH (001) systems. The work function is given by the difference between the Fermi energy and the value of the one-electron potential in vacuum. Vacuum is reached as the potential does not change anymore with increasing distance from the surface. As shown in Fig 7 (a), for the bare β-$Ni(OH)_2$ (001) calculation of the work function yields a value of 3.87 eV. This value agrees well with the reported experimental value of the work function, which is 3.7 eV [59]. The presence of a water layer in H-down configuration increases the work function to 4.62 eV; while a water layer in H-up configuration causes a decrease to 3.02 eV. The opposite trends are expected due to the opposite dipole moments of the two water layers normal to the surface [39].

For the bare β-NiOOH (001) surface the work function was found to be 5.18 eV. The reported experimental value of work function for this surface is 5.3 eV [60]. Upon adsorption of the H-down water layer the work function shifts to 5.56 eV. As discussed, the H-down configuration is strongly preferred on this surface due to the favorable formation of hydrogen bonds between the water molecules and O^{ad} at the surface.

In comparison to β-$Ni(OH)_2$ (001), we first notice the significant increase in the work function for the β-NiOOH surface. Additionally, we notice that the increase in the work function for β-NiOOH (001),

View Article Online
DOI: 10.1039/C7CP03396F

caused by the adsorption of H-down water layer, is smaller than that for β-$Ni(OH)_2$ (001); this effect is due to the larger dipole-dipole interaction of water with the β-NiOOH (001) surface and the overall tendency to keep the work function lower for this system, as also discussed in ref. [39] for close-packed transition metal surfaces.

The thermal fluctuations of the surface water layers have been explored by AIMD simulations at a temperature of 140 K for a run time of 5 ps (5000 time steps). Initial structures were chosen as the optimized water structures at 2/3 ML coverage with maximum hydrogen bond network, as shown in in Fig. 2 (f), (r), and (x).

The structure of water at β-$Ni(OH)_2$ and β-NiOOH (001) surfaces at t = 5 ps is depicted in Fig. 8 with the lower panel showing the trajectories of oxygen atoms of the water molecules during the molecular dynamics simulation run. A visual comparison shows indications of disorder in the water structure at β-$Ni(OH)_2$. For example, we can observe the deviation of the water structure from the closed hexagon. On the other hand, we do not observe a significant structural reorganization on β-Ni(OOH) (001), irrespective of the surface termination for this case.

We have plotted distribution functions for the distance of the oxygen atoms in the water layer from the β-$Ni(OH)_2$ and β-NiOOH (001) surfaces. This enables us to observe the extent at which the water molecules are displaced from the surface over the simulation run. As shown in Fig. 9, a decrease in peak height and increase in the distribution spread is found as we go from β-NiOOH (001) to β-$Ni(OH)_2$ (001), indicating the increased disorder in the water layer for the latter system. Moreover, the closer proximity of the water molecules to β-NiOOH (001) as well as the sharper distribution reflect the stronger water-surface interaction on this surface as compared to β-$Ni(OH)_2$ (001).

Next, we further increased the coverage by introducing extra water molecules to the unit cell. The resulting interactions between the water molecules weaken the interaction of individual water molecules with the surface; consequently, a shift of the position of water from the surface should be observed. In

View Article Online
DOI: 10.1039/C7CP03396F

this case, the water coverage was increased to 1 ML for β-$Ni(OH)_2$ (001) and 5/6 ML for β-NiOOH (001) so that the total number of water molecules per surface area is almost the same for both systems. Fig. 10 (a) shows the side and top views of the trajectory paths of oxygen atoms in the water layer. It is obvious that the water molecules are highly mobile and disordered on β-$Ni(OH)_2$ (001), while their mobility is suppressed on β-NiOOH (001) due to the stability of the ordered sheet of water on this surface. Fig. 10 (b) compares the corresponding oxygen-wall distribution for the coverage of 1 ML water on β-$Ni(OH)_2$ (001) and 5/6 ML for β-NiOOH (001) over the simulation run of 3 ps. As can be seen the presence of extra water molecules leads to a shift of weakly adsorbed water molecules away from the surface of β-$Ni(OH)_2$ (001). On the other hand, the strong interaction of water with β-NiOOH (001), as well as the strong water-water interaction on this surface, keeps the water distribution highly localized and the regular arrangement intact for this surface.

A recent experimental study by Chang *et al.* supports our results [61]. The authors of that article explored the switchable wettability of amorphous and nanoporous NiOOH/$Ni(OH)_2$. While the as-prepared NiOOH film exhibits hydrophilic characteristics (with a wetting angle of 6.9 ± 1°), exposure to an environmental chamber with 85° C, %70 RH transforms the film towards becoming transparent and hydrophobic with a wetting angle of 138.9 ± 3° [61]. As confirmed by high-resolution transmission electron microscopy (HR-TEM) in their study, the conditioning in the environmental chamber induces a transition from the γ-NiOOH phase to the α-$Ni(OH)_2$ phase. Furthermore, a X-ray photoelectron spectroscopy (XPS) analysis performed in that work revealed that the peak associated with water adsorption on NiOOH disappears upon phase transition to $Ni(OH)_2$. It was scrutinized that the nanoporous structure for NiOOH and $Ni(OH)_2$ remained the same. Therefore, changes in wettability should be ascribed to specific surface effects. In an electrochemical environment, another way to induce the phase transition between hydrophilic NiOOH and hydrophobic $Ni(OH)_2$ would be to change the

View Article Online
DOI: 10.1039/C7CP03396F

electrode potential. The presented work can be extended to study the wettability of other related systems, including α-$Ni(OH)_2$ and γ NiOOH phases as well as ultrathin Ni (hydroxy)oxide films [62].

4. CONCLUSIONS

We studied the adsorption of water on β-$Ni(OH)_2$ (001) and β-NiOOH (001) by means of first principles calculations. It was found that water interacts weakly with β-$Ni(OH)_2$ (001) but rather strongly with β-NiOOH (001) surfaces. The weaker interaction of water with β-$Ni(OH)_2$ (001) results in a highly disordered water structure as seen in AIMD simulations; in contrast, a highly ordered water structure was observed on β-NiOOH (001). The stronger interaction of water with Ni oxyhydroxides was found to be due to the much larger dipole moment of this surface relative to Ni hydroxide; in addition, the presence of unsaturated O^{ad} on Ni oxyhydroxides results in the formation of more hydrogen bonds with surficial water molecules This opposite wettability behavior for the two surfaces has been also addressed in a recent experimental work suggesting that β-$Ni(OH)_2$ has a hydrophobic nature, while β-NiOOH (001) has a hydrophilic nature. Moreover, calculated work function values for the two surfaces were in agreement with the experimental data available in the literature indicating a significant upshift from β-$Ni(OH)_2$ (001) to β-NiOOH (001).

ACKNOWLEDGMENT

This research was conducted as part of the Engineered Nickel Catalysts for Electrochemical Clean Energy project administered from Queen's University and supported by Grant No. RGPNM 477963-2015 under the Natural Sciences and Engineering Research Council of Canada (NSERC) Discovery Frontiers Program. MJE thanks the Institute of Theoretical Chemistry at Ulm University for providing support for his stay at Ulm University as a guest scientist through grant GR 1503/23-2 of the German Science Foundation (DFG) within the Research Unit FOR 1376. Furthermore, MJE wish to acknowledge useful discussions with Dr. Sung Sakong and Dr. Jan Kucera.

View Article Online
DOI: 10.1039/C7CP03396F

REFERENCES

[1] S. Dutta, A review on production, storage of hydrogen and its utilization as an energy resource, *J. Ind. Eng. Chem*. 2014, **20**, 1148-56.

[2] N.T. Suen, S. F. Hung, Q. Quan, N. Zhang, Y. J. Xu, H. M. Chen, Electrocatalysis for the oxygen evolution reaction: recent development and future perspectives, *Chem. Soc. Rev*. 2017, **46**, 337-65.

[3] M. Carmo, D. L. Fritz, J. Mergel, D. Stolten, A comprehensive review on PEM water electrolysis. International journal of hydrogen energy, *Int. J. Hydrogen Energy*. 2013, **38**, 4901-34.

[4] L. Trotochaud, J. K. Ranney, K. N. Williams, S. W. Boettcher, Solution-cast metal oxide thin film electrocatalysts for oxygen evolution, *J. Am. Chem. Soc.* 2012, **134**, 17253-61.

[5] P. Du, R. Eisenberg, Catalysts made of earth-abundant elements (Co, Ni, Fe) for water splitting: recent progress and future challenges, *Energy Environ. Sci*. 2012, **5**, 6012-21.

[6] M. Gao, W. Sheng, Z. Zhuang, Q. Fang, S. Gu, J. Jiang, Y. Yan, Efficient water oxidation using nanostructured α-nickel-hydroxide as an electrocatalyst, *J. Am. Chem. Soc.* 2014, **136**, 7077-84.

[7] K. Fominykh, P. Chernev, I. Zaharieva, J. Sicklinger, G. Stefanic, M. Döblinger, A. Müller, A. Pokharel, S. Böcklein, C. Scheu, T. Bein, Iron-doped nickel oxide nanocrystals as highly efficient electrocatalysts for alkaline water splitting, *ACS Nano*. 2015, **9**, 5180-8.

[8] P. Oliva, J. Leonardi, J. F. Laurent, C. Delmas, J. J. Braconnier, M. Figlarz, F. Fievet, A. De Guibert, Review of the structure and the electrochemistry of nickel hydroxides and oxy-hydroxides, *J. Power Sources*, 1982, **8**, 229-55.

[9] D. S. Hall, D. J. Lockwood, C. Bock, B. R. MacDougall, Nickel hydroxides and related materials: a review of their structures, synthesis and properties, *InProc. R. Soc. A*. 2015, **471**, 20140792.

View Article Online
DOI: 10.1039/C7CP03396F

[10] L. Trotochaud, S. L. Young, J. K. Ranney, S. W. Boettcher, Nickel–iron oxyhydroxide oxygen-evolution electrocatalysts: the role of intentional and incidental iron incorporation, *J. Am. Chem. Soc.* 2014, **136**, 6744-53.

[11] K. Fan, H. Chen, Y. Ji, H. Huang, P. M. Claesson, Q. Daniel, B. Philippe, H. Rensmo, F. Li, Y. Luo, L. Sun, Nickel-vanadium monolayer double hydroxide for efficient electrochemical water oxidation, *Nat. Commun*. 2016, **7**, DOI: 10.1038/ncomms11981.

[12] O. Diaz-Morales, D. Ferrus-Suspedra, M. T. Koper, The importance of nickel oxyhydroxide deprotonation on its activity towards electrochemical water oxidation, *Chem. Sci*. 2016, **7**, 2639-45.

[13] H. Bode, K. Dehmelt, J. Witte, Zur kenntnis der nickelhydroxidelektrode—I. Über das nickel (II)-hydroxidhydrat *, Electrochim. Acta*. 1966, **11**, 1079IN1-87.

[14] M. Alsabet, M. Grden, G. Jerkiewicz, Electrochemical growth of surface oxides on nickel. Part 1: formation of α-Ni (OH) 2 in relation to the polarization potential; polarization time, and temperature, *Electrocatal*. 2011, **2**, 317-30.

[15] M. Alsabet, M. Grden, G. Jerkiewicz, Electrochemical growth of surface oxides on nickel. Part 2: formation of β-Ni (OH) 2 and NiO in relation to the polarization potential, polarization time, and temperature, *Electrocatal*. 2014, **5**, 136-47.

[16] M. Alsabet, M. Grdeń, G. Jerkiewicz, Electrochemical growth of surface oxides on nickel. Part 3: Formation of β-NiOOH in relation to the polarization potential, polarization time, and temperature, *Electrocatal*. 2015, **6**, 60-71.

[17] R. S. McEwen, Crystallographic studies on nickel hydroxide and the higher nickel oxides, *J. Phys. Chem.* 1971, **75**, 1782-9.

View Article Online
DOI: 10.1039/C7CP03396F

[18] V. Y. Kazimirov, M. B. Smirnov, L. Bourgeois, L. Guerlou-Demourgues, L. Servant, A. M. Balagurov, I. Natkaniec, N. R. Khasanova, E. V. Antipov, Atomic structure and lattice dynamics of Ni and Mg hydroxides, *Solid State Ion*. 2010, **181**, 1764-70.

[19] Q. Song, Z. Tang, H. Guo, S. L. Chan, Structural characteristics of nickel hydroxide synthesized by a chemical precipitation route under different pH values, *J. Power Sources*. 2002, **112**, 428-34.

[20] A. J. Tkalych, K. Yu, E. A. Carter, Structural and electronic features of β-Ni (OH) 2 and β-NiOOH from first principles, *J. Phys. Chem. C*. 2015, **119**, 24315-22.

[21] J. C. Conesa, Electronic Structure of the (Undoped and Fe-Doped) NiOOH O2 Evolution Electrocatalyst, *J. Phys. Chem. C*. 2016, **120**, 18999-9010.

[22] Y. F. Li, A. Selloni, Mechanism and activity of water oxidation on selected surfaces of pure and Fe-doped NiOx, *ACS Catal*. 2014, **4**, 1148-53.

[23] D. Friebel, M. W. Louie, M. Bajdich, K. E. Sanwald, Y. Cai, A. M. Wise, M. J. Cheng, D. Sokaras, T. C. Weng, R. Alonso-Mori, R. C. Davis, Identification of highly active Fe sites in (Ni, Fe) OOH for electrocatalytic water splitting, *J. Am. Chem. Soc.*. 2015, **137**, 1305-13.

[24] O. Diaz-Morales, I. Ledezma-Yanez, M. T. Koper, F. Calle-Vallejo, Guidelines for the rational design of Ni-based double hydroxide electrocatalysts for the oxygen evolution reaction, *ACS Catal.* 2015, **5**, 5380–5387

[25] V. Fidelsky, M. C. Toroker, Enhanced Water Oxidation Catalysis of Nickel Oxyhydroxide through the Addition of Vacancies, *J. Phys. Chem. C*. 2016, **120**, 25405-10.

[26] V. Fidelsky, M. Caspary Toroker, Engineering Band Edge Positions of Nickel Oxyhydroxide through Facet Selection, *J. Phys. Chem. C*. 2016, **120**, 8104-8.

View Article Online
DOI: 10.1039/C7CP03396F

[27] Z. Zeng, M. K. Chan, Z. J. Zhao, J. Kubal, D. Fan, J. Greeley, Towards first principles-based prediction of highly accurate electrochemical Pourbaix diagrams, *J. Phys. Chem. C*. 2015, **119**, 18177-87.

[28] M. J. Eslamibidgoli, J. Huang, T. Kadyk, A. Malek, M. Eikerling, How theory and simulation can drive fuel cell electrocatalysis, *Nano Energy*. 2016, **29**, 334-61.

[29] S. Sakong, K. Forster-Tonigold, A. Groß, The structure of water at a Pt (111) electrode and the potential of zero charge studied from first principles, *J. Chem. Phys*. 2016, **144**, 194701.

[30] J. Fester, M. García-Melchor, A. S. Walton, M. Bajdich, Z. Li, L. Lammich, A. Vojvodic, J. V. Lauritsen, Edge reactivity and water-assisted dissociation on cobalt oxide nanoislands, *Nat. Commun.* 2017, **8**, doi:10.1038/ncomms14169.

[31] M. J. Eslamibidgoli, M. H. Eikerling, Electrochemical Formation of Reactive Oxygen Species at Pt (111) - A Density Functional Theory Study, *ACS Catal*. 2015, **5**, 6090-8.

[32] K. A. Stoerzinger, W. T. Hong, G. Azimi, L. Giordano, Y. L. Lee, E. J. Crumlin, M. D. Biegalski, H. Bluhm, K. K. Varanasi, Y. Shao-Horn, Reactivity of perovskites with water: role of hydroxylation in wetting and implications for oxygen electrocatalysis, *J. Phys. Chem. C*. 2015, **119**, 18504-12.

[33] C. Meng, B. Wang, Z. Gao, Z. Liu, Q. Zhang, J. Zhai, Insight into the Role of Surface Wettability in Electrocatalytic Hydrogen Evolution Reactions Using Light-Sensitive Nanotubular TiO2 Supported Pt Electrodes, *Sci. Rep*. 2017, **7**, doi: 10.1038/srep41825.

[34] S. Liu, M. G. White, P. Liu, Mechanism of oxygen reduction reaction on Pt (111) in alkaline solution: Importance of chemisorbed water on surface, *J. Phys. Chem. C*. 2016, **120**, 15288-98.

[35] V. Tripković, E. Skúlason, S. Siahrostami, J. K. Nørskov, J. Rossmeisl, The oxygen reduction reaction mechanism on Pt (111) from density functional theory calculations, *Electrochim. Acta*. 2010, **55**, 7975-81.

View Article Online
DOI: 10.1039/C7CP03396F

[36] H. F. Wang, Z. P. Liu, Formic acid oxidation at Pt/H2O interface from periodic DFT calculations integrated with a continuum solvation model, *J. Phys. Chem. C*. 2009, **113**, 17502-8.

[37] I. Ledezma-Yanez, W. D. Wallace, P. Sebastián-Pascual, V. Climent, J. M. Feliu, M. T. Koper, Interfacial water reorganization as a pH-dependent descriptor of the hydrogen evolution rate on platinum electrodes, *Nature Energy*. 2017, **2**, 17031.

[38] J. Huang, A. Malek, J. Zhang, M. H. Eikerling, Non-monotonic Surface Charging Behavior of Platinum: A Paradigm Change, *J. Phys. Chem. C*. 2016, **120**, 13587-95.

[39] S. Schnur, A. Groß, Properties of metal–water interfaces studied from first principles, *New J. Phys*. 2009, **11**, 125003.

[40] A. Groß, F. Gossenberger, X. Lin, M. Naderian, S. Sakong, T. Roman, Water structures at metal electrodes studied by ab initio molecular dynamics simulations, *J. Electrochem. Soc.* 2014, **161**, E3015-20.

[41] X. Lin, F. Evers, A. Groß, First-principles study of the structure of water layers on flat and stepped Pb electrodes, *Beilstein J. Nanotechnol*. 2016, **7**, 533-43.

[42] T. Roman, A. Groß, Structure of water layers on hydrogen-covered Pt electrodes, *Catal Today*. 2013, **202**, 183-90.

[43] J. M. Fischer, D. Mahlberg, T. Roman, A. Groß, Water adsorption on bimetallic PtRu/Pt (111) surface alloys, *InProc. R. Soc. A,* 2016, **472**, 20160618.

[44] M. Naderian, A. Groß, From single molecules to water networks: Dynamics of water adsorption on Pt (111), *J. Chem. Phys.* 2016, **145**, 094703.

[45] X. Lin, A. Groß, First-principles study of the water structure on flat and stepped gold surfaces, *Surf. Sci*. 2012, **606**, 886-91.

View Article Online
DOI: 10.1039/C7CP03396F

[46] G. Kresse, J. Furthmüller, Efficient iterative schemes for ab initio total-energy calculations using a plane-wave basis set, *Phys. Rev. B*. 1996, **54**, 11169.

[47] G. Kresse, J. Furthmüller, Efficiency of ab-initio total energy calculations for metals and semiconductors using a plane-wave basis set, *Comput. Mater. Sci*. 1996, **6**, 15-50.

[48] P. E. Blöchl, Projector augmented-wave method, *Phys. Rev. B*. 1994, **50**, 17953.

[49] J. P. Perdew, K. Burke, M. Ernzerhof, Generalized gradient approximation made simple, *Phys. Rev. Lett*. 1996, **77**, 3865.

[50] A. J. Cohen, P. Mori-Sánchez, W. Yang W. Insights into current limitations of density functional theory, *Sci*. 2008, **321**, 792-4.

[51] S. L. Dudarev, G. A. Botton, S. Y. Savrasov, C. J. Humphreys, A. P. Sutton, Electron-energy-loss spectra and the structural stability of nickel oxide: An LSDA+ U study, *Phys. Rev. B*. 1998, **57**, 1505.

[52] M. Cococcioni, S. De Gironcoli, Linear response approach to the calculation of the effective interaction parameters in the LDA+ U method, *Phys. Rev. B*. 2005, **71**, 035105.

[53] A. Van der Ven, D. Morgan, Y. S. Meng, G. Ceder, Phase stability of nickel hydroxides and oxyhydroxides, *J. Electrochem. Soc.*. 2006, **153**, A210-5.

[54] H. J. Monkhorst, J. D. Pack, Special points for Brillouin-zone integrations, *Phys. Rev. B*. 1976, **13**, 5188.

[55] F. P. Kober, Analysis of the Charge-Discharge Characteristics of Nickel-Oxide Electrodes by Infrared Spectroscopy, *J. Electrochem. Soc.* 1965, **112**, 1064-7.

[56] P. A. Thiel, T. E. Madey, The interaction of water with solid surfaces: Fundamental aspects*, Surf. Sci Rep*. 1987, **7**, 211-385.

View Article Online
DOI: 10.1039/C7CP03396F

[57] A. Roudgar, A. Groß, Water bilayer on the Pd/Au (111) overlayer system: Coadsorption and electric field effects, *Chem. Phys. Lett*. 2005, **409**, 157-62.

[58] K. Tonigold, A. Groß, Dispersive interactions in water bilayers at metallic surfaces: A comparison of the PBE and RPBE functional including semiempirical dispersion corrections, *J. Comput. Chem.* 2012**, 33**, 695-701.

[59] H. W. Hoppe, H. H. Strehblow, XPS and UPS examinations of the formation of passive layers on Ni in 1 M sodium hydroxide and 0.5 M sulphuric acid, *Surf. Interface Anal*. 1989, **14**, 121-31.

[60] E. L. Ratcliff, J. Meyer, K. X. Steirer, A. Garcia, J. J. Berry, D. S. Ginley, D. C. Olson, A. Kahn, N. R. Armstrong, Evidence for near-surface NiOOH species in solution-processed NiO x selective interlayer materials: impact on energetics and the performance of polymer bulk heterojunction photovoltaics, *Chem. Mater*. 2011, **23**, 4988-5000.

[61] Y. H. Chang, N. Y. Hau, C. Liu, Y. T. Huang, C. C. Li, K. Shih, S. P. Feng, A short-range ordered–disordered transition of a NiOOH/Ni (OH) $_2$ pair induces switchable wettability, *Nanoscale*. 2014, **6**, 15309-15.

[62] Z. Zeng, K-C Chang, J. Kubal, N. M. Markovic, J. Greeley, Stabilization of ultrathin (hydroxy) oxide films on transition metal substrates for electrochemical energy conversion, Nat. Energy. 2017, **2,** 17070.

View Article Online
DOI: 10.1039/C7CP03396F

Table 1 Various water monomer configurations on the studied surfaces and their calculated adsorption energies

Surface configuration	**Water monomer configuration**	**E_{ad} (eV)**
β-$Ni(OH)_2$ (001)	Flat-lying above Ni atom	-0.06
β-$Ni(OH)_2$ (001)	Flat-lying above OH^{ad}	-0.09
β-$Ni(OH)_2$ (001)	Tilted H-down above Ni atom (Initial configuration: H-up above Ni atom)	-0.25
β-$Ni(OH)_2$ (001)	H-down above Ni atom	-0.21
β-$Ni(OH)_2$ (001)	Tilted above OH^{ad} (Initial configuration: H-up above OH^{ad})	-0.11
β-$NiOOH_{25/75}$ (001)	Tilted above OH^{ad} (Initial configuration: H-down above O^{ad})	-0.45
β-$NiOOH_{25/75}$ (001)	Tilted above OH^{ad} (Initial configuration: Flat-lying on OH^{ad})	-0.45
β-$NiOOH_{50/50}$ (001)	H-down above O^{ad}	-0.39
β-$NiOOH_{50/50}$ (001)	Tilted above OH^{ad}	-0.54
β-$NiOOH_{75/25}$ (001)	H-down above O^{ad}	-0.69

View Article Online
DOI: 10.1039/C7CP03396F

β-$NiOOH_{75/25}$ (001)	H-down above O^{ad} (Initial configuration: H-down above Ni)	-0.69
β-$NiOOH_{75/25}$ (001)	Flat-lying above OH^{ad}	-0.17

FIGURE CAPTIONS

Figure 1 Model used for the calculations. The top panel shows unit cells and parameters of bulk crystal structures of (a) β-$Ni(OH)_2$ and (b) β-NiOOH. The bottom panel shows top view of (c) β-$Ni(OH)_2$ (001), (d) β-NiOOH (001) terminated with 25% OH – 75% O, (e) β-NiOOH (001) terminated with 50% OH – 50% O and (f) β-NiOOH (001) terminated with 75% OH – 25% O. Grey, red and white colors are used to represent Ni, O and H atoms, respectively.

Figure 2 Water monomer adsorption and most stable configuration on various NiO_x (001) surfaces

Figure 3 Calculated coverage dependent water adsorption energies for (a)-(f) β-$Ni(OH)_2$ (001), (g)-(i) β-NiOOH (001) terminated with 25% OH – 75% O, (m)-(r) β-NiOOH (001) terminated with 50% OH – 50% O and (s)-(x) β-NiOOH (001) terminated with 75% OH – 25% O. Grey, red, blue and white colors are used to represent Ni, O in nickel (oxy)hydroxides, O in water and H atoms, respectively.

Figure 4 Calculated adsorption energies of the H-down water structure on Ni (oxy)hydroxide (001) surfaces studied in this work. For comparison the lattice energy of bulk ice per molecule is shown.

Figure 5 Electron density difference profile along z direction for (a) β-$Ni(OH)_2$ (001), (b) β-$NiOOH_{50/50}$ (001), (c) β-$NiOOH_{25/75}$ and β-$NiOOH_{75/25}$ (001). Calculated surface dipole moments were shown for each surface.

View Article Online
DOI: 10.1039/C7CP03396F

Figure 6 (a) and (b) Isosurface plots of charge-density differences upon water adsorption on β-$Ni(OH)_2$ (001) and β-NiOOH (001), respectively. The plotted isosurfaces correspond to charge density with an absolute value of 0.002 e/$Å^2$. Charge accumulation zone, i.e., an increase in the electron density, is plotted in yellow, and charge depletion zone in blue. (c) and (d) Averaged charge-density differences along the surface normal for the adsorption of water on β-$Ni(OH)_2$ (001) and β-NiOOH (001), respectively.

Figure 7 One-electron potential averaged in lateral direction as a function of the position along the surface normal for symmetric water adsorption on (a) β-$Ni(OH)_2$ (001) slab and (b) β-NiOOH (001) slab terminated with 50% OH-50% O. Calculated work function values are included and compared to reported experimental values [59, 60]

Figure 8 Snapshots of the side and the top views of the structure of water bilayer taken from the AIMD simulations of water at 140 K on β-$Ni(OH)_2$ (001), β-NiOOH (001) terminated with 50% OH-50% O, and β-NiOOH (001) terminated with 75% OH – 25% O. Lower panel: trajectories of the oxygen atoms of the water molecules along the AIMD run indicated by different color lines. The water coverages correspond to 2/3 ML.

Figure 9 Wall–oxygen distribution function obtained from the AIMD simulations for the system with 2/3 ML water on nickel (oxy)hydroxide (001)

Figure 10 (a) Side and top views of the trajectories of the oxygen atoms of water molecules during the AIMD run at 140 K on indicated by different color lines. The water coverages correspond to 1 ML at (a) β-$Ni(OH)_2$ (001) and (b) 5/6 ML at β-NiOOH (001) terminated with 50% OH-50% O. (b) Wall–oxygen distribution function obtained from the AIMD simulations of 1 ML water on β-$Ni(OH)_2$ (001) and 5/6 ML water on β-NiOOH (001).

View Article Online
DOI: 10.1039/C7CP03396F

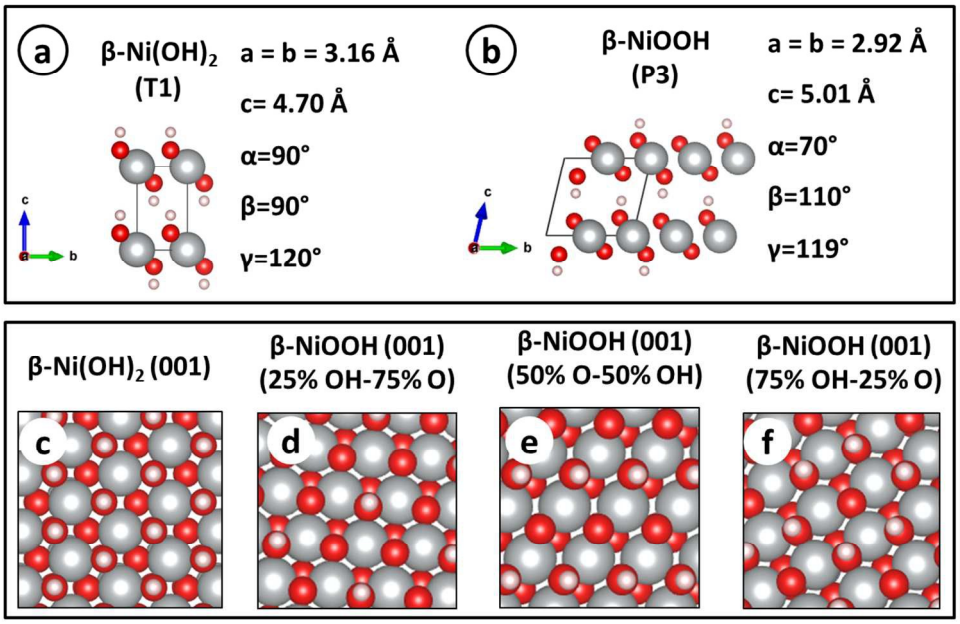

Figure 1 Model used for the calculations. The top panel shows unit cells and parameters of bulk crystal structures of (a) β-Ni(OH)2 and (b) β-NiOOH. The bottom panel shows top view of (c) β-Ni(OH)2 (001), (d) β-NiOOH (001) terminated with 25% OH – 75% O, (e) β-NiOOH (001) terminated with 50% OH – 50% O and (f) β-NiOOH (001) terminated with 75% OH – 25% O. Grey, red and white colors are used to represent Ni, O and H atoms, respectively.

222x145mm (150 x 150 DPI)

View Article Online
DOI: 10.1039/C7CP03396F

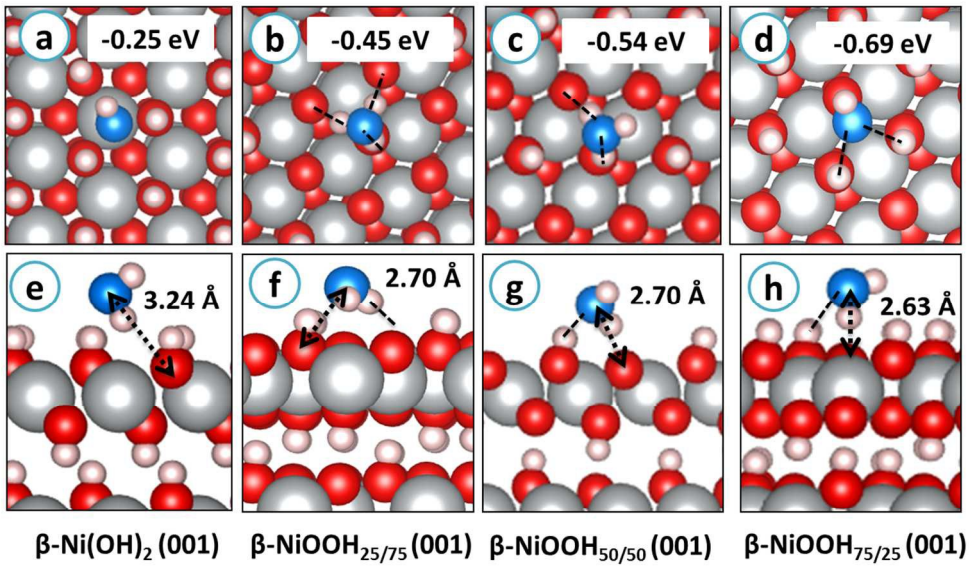

Figure 2 Water monomer adsorption and most stable configuration on various NiOx (001) surfaces

220x135mm (150 x 150 DPI)

View Article Online
DOI: 10.1039/C7CP03396F

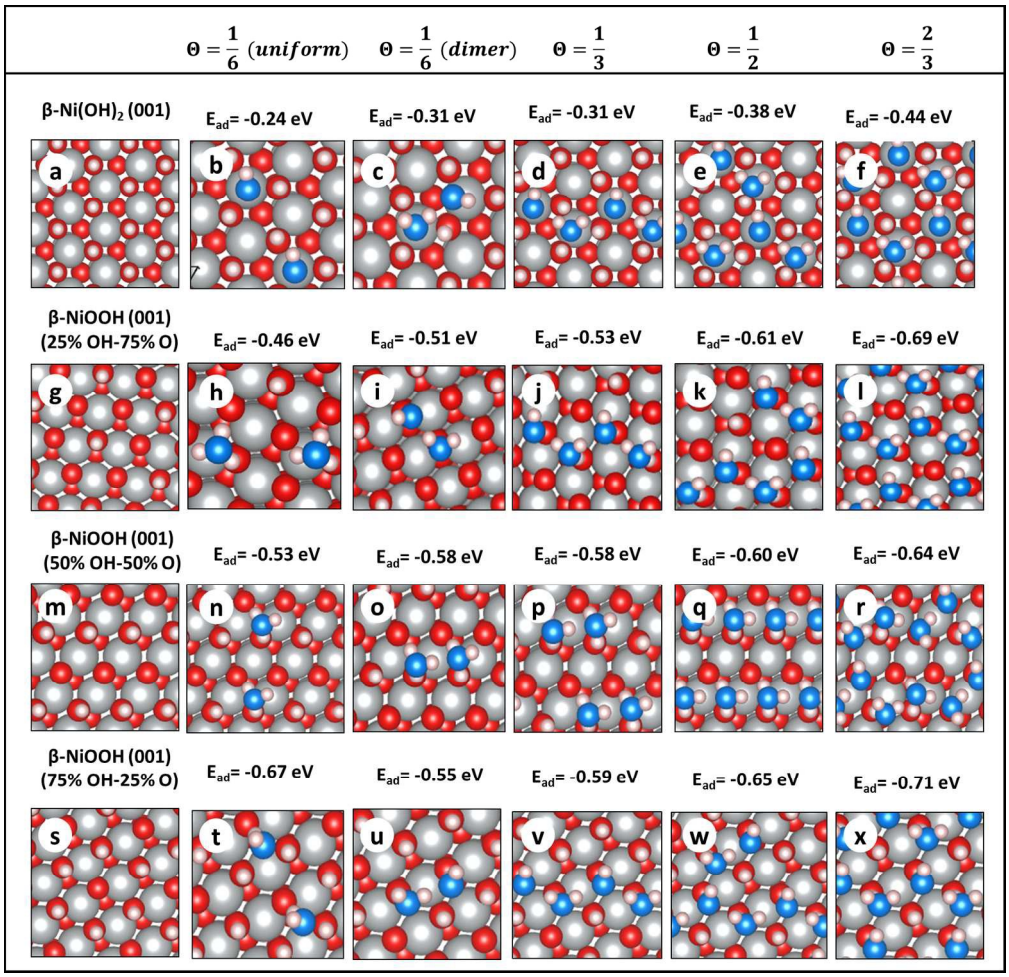

Figure 3 Calculated coverage dependent water adsorption energies for (a)-(f) β-Ni(OH)2 (001), (g)-(i) β-NiOOH (001) terminated with 25% OH – 75% O, (m)-(r) β-NiOOH (001) terminated with 50% OH – 50% O and (s)-(x) β-NiOOH (001) terminated with 75% OH – 25% O. Grey, red, blue and white colors are used to represent Ni, O in nickel (oxy)hydroxides, O in water and H atoms, respectively.

316x305mm (150 x 150 DPI)

View Article Online
DOI: 10.1039/C7CP03396F

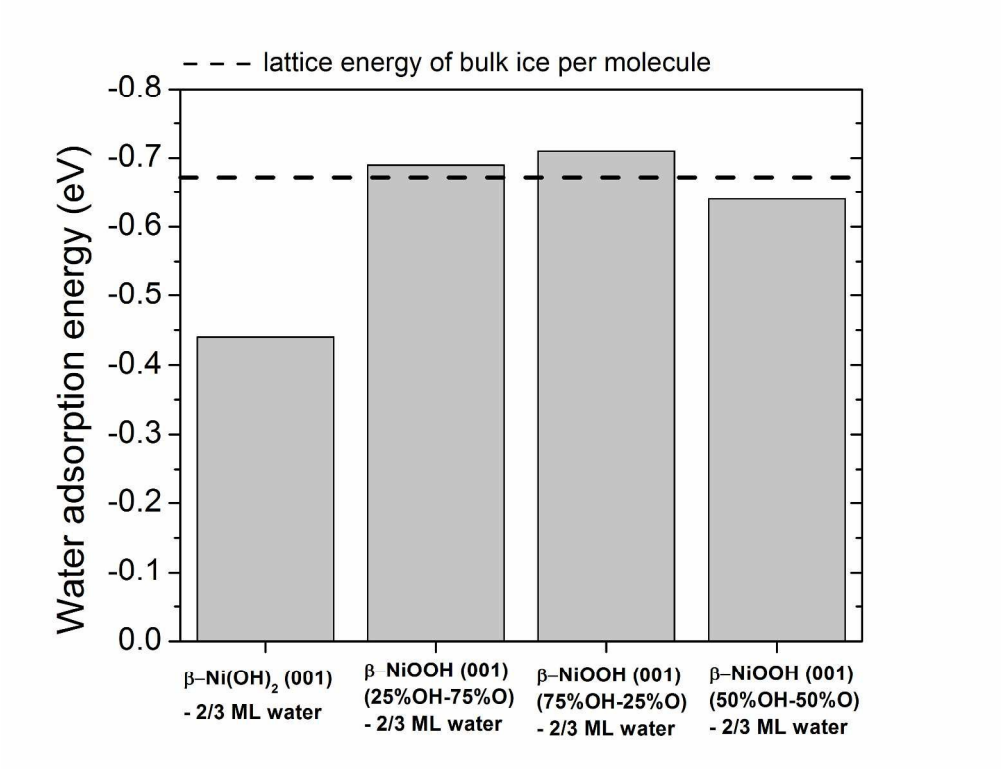

Figure 4 Calculated adsorption energies of the H-down water structure on Ni (oxy)hydroxide (001) surfaces studied in this work. For comparison the lattice energy of bulk ice per molecule is shown.

269x207mm (300 x 300 DPI)

View Article Online
DOI: 10.1039/C7CP03396F

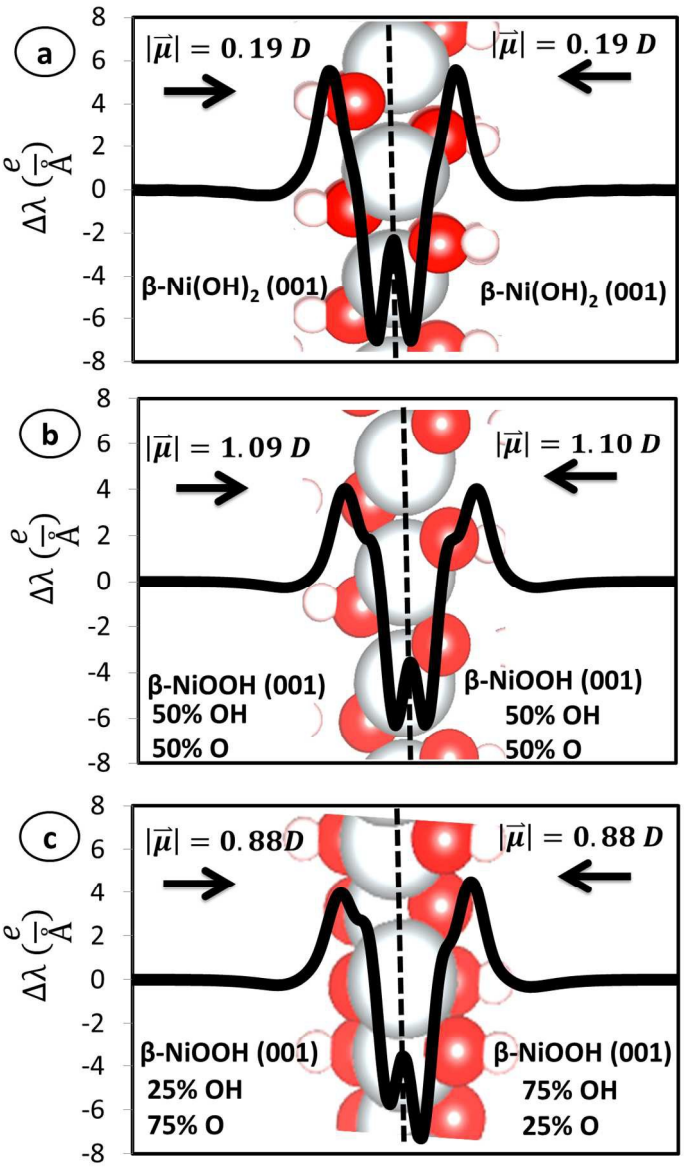

Figure 5 Electron density difference profile along z direction for (a) β-Ni(OH)2 (001), (b) β-NiOOH50/50 (001), (c) β-NiOOH25/75 and β-NiOOH75/25 (001). Calculated surface dipole moments were shown for each surface.

206x345mm (150 x 150 DPI)

View Article Online
DOI: 10.1039/C7CP03396F

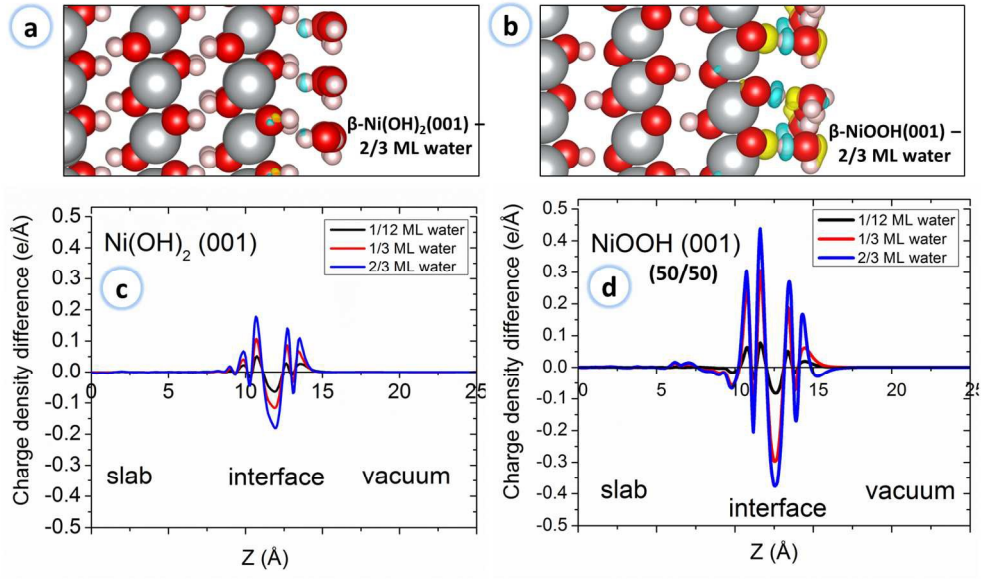

Figure 6 (a) and (b) Isosurface plots of charge-density differences upon water adsorption on β-Ni(OH)2 (001) and β-NiOOH (001), respectively. The plotted isosurfaces correspond to charge density with an absolute value of 0.002 e/Å2. Charge accumulation zone, i.e., an increase in the electron density, is plotted in yellow, and charge depletion zone in blue. (c) and (d) Averaged charge-density differences along the surface normal for the adsorption of water on β-Ni(OH)2 (001) and β-NiOOH (001), respectively.

282x174mm (150 x 150 DPI)

View Article Online
DOI: 10.1039/C7CP03396F

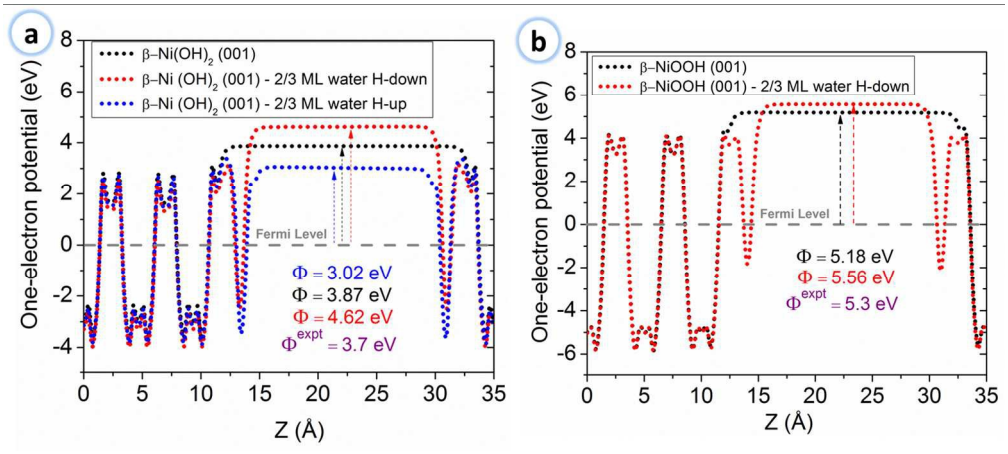

Figure 7 One-electron potential averaged in lateral direction as a function of the position along the surface normal for symmetric water adsorption on (a) β-Ni(OH)2 (001) slab and (b) β-NiOOH (001) slab terminated with 50% OH-50% O. Calculated work function values are included and compared to reported experimental values [59, 60]

271x123mm (150 x 150 DPI)

View Article Online
DOI: 10.1039/C7CP03396F

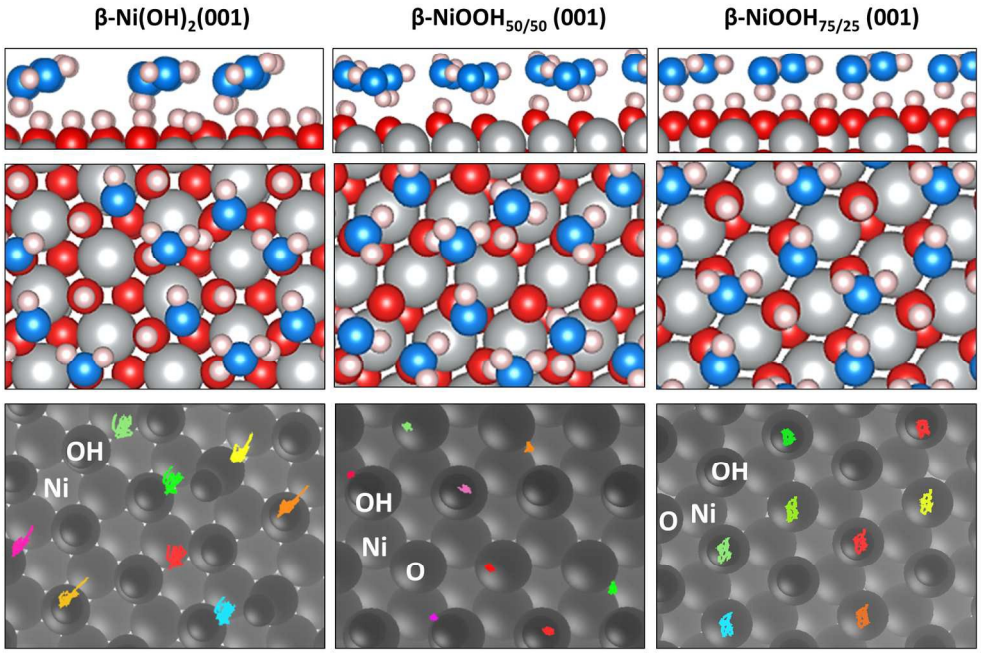

Figure 8 Snapshots of the side and the top views of the structure of water bilayer taken from the AIMD simulations of water at 140 K on β-Ni(OH)2 (001), β-NiOOH (001) terminated with 50% OH-50% O, and β-NiOOH (001) terminated with 75% OH – 25% O. Lower panel: trajectories of the oxygen atoms of the water molecules along the AIMD run indicated by different color lines. The water coverages correspond to 2/3 ML.

335x239mm (150 x 150 DPI)

View Article Online
DOI: 10.1039/C7CP03396F

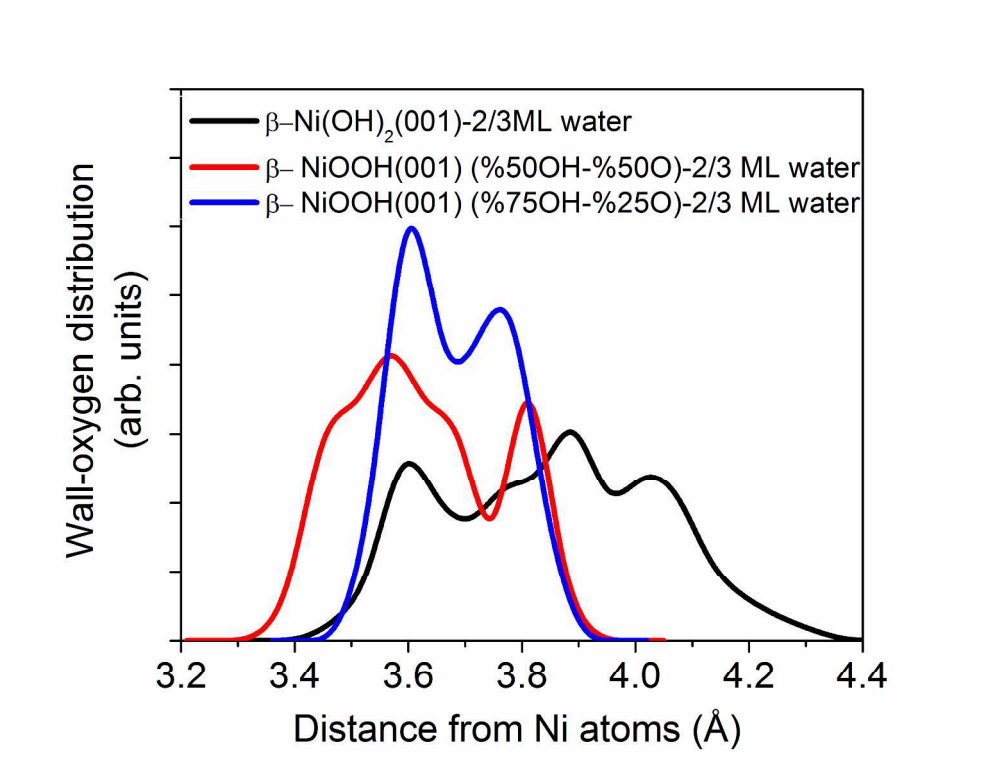

Figure 9 Wall–oxygen distribution function obtained from the AIMD simulations for the system with 2/3 ML water on nickel (oxy)hydroxide (001)

269x207mm (300 x 300 DPI)

View Article Online
DOI: 10.1039/C7CP03396F

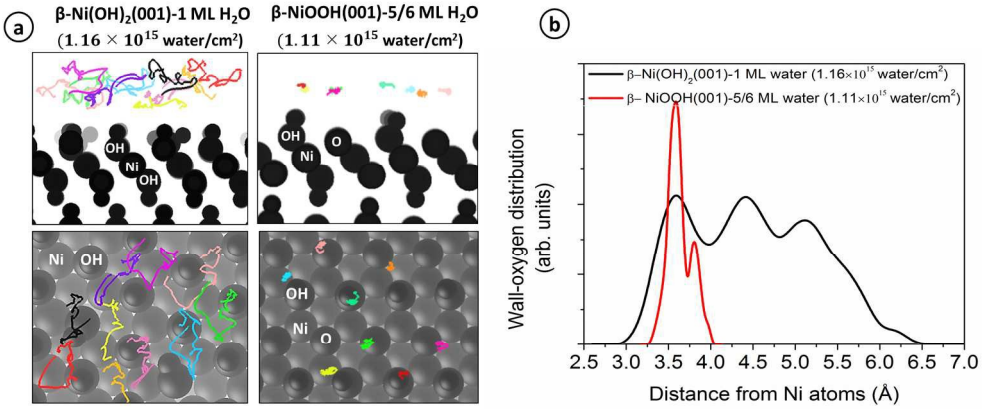

Figure 10 (a) Side and top views of the trajectories of the oxygen atoms of water molecules during the AIMD run at 140 K on indicated by different color lines. The water coverages correspond to 1 ML at (a) β-Ni(OH)2 (001) and (b) 5/6 ML at β-NiOOH (001) terminated with 50% OH-50% O. (b) Wall–oxygen distribution function obtained from the AIMD simulations of 1 ML water on β-Ni(OH)2 (001) and 5/6 ML water on β-NiOOH (001).

375x167mm (150 x 150 DPI)